Monitoring Fracture of Steel Corroded Reinforced Concrete Members under Flexure by Acoustic Emission Technique

Elsevier Editorial System(tm) for
Construction & Building Materials
Manuscript Draft

Manuscript Number: CONBUILDMAT-D-16-03871R1

Title: Monitoring Fracture of Steel Corroded Reinforced Concrete Members under Flexure by Acoustic Emission Technique

Article Type: VSI:ETNDT6

Keywords: Acoustic emission; steel corrosion; Damage probability function; Reinforced concrete; Weibull distribution; Concrete fracture monitoring

Corresponding Author: Dr. Hwa Kian Chai,

Corresponding Author's Institution:

First Author: Ahmad Zaki

Order of Authors: Ahmad Zaki; Hwa Kian Chai; Arash Behnia; Dimitrios G. Aggelis; Jun Ying Tan; Zainah Ibrahim

Abstract: Acoustic emission (AE) technique is used for monitoring and evaluating the influence of corrosion on the structural behaviour of steel reinforced concrete (RC) beams under three-point flexure test. In this study, steel corrosion was accelerated by electro-chemical method utilising a direct current (DC) power supply and 5% sodium chloride (NaCl) solution. The steel corrosion that was induced into beam specimens casting were estimated at 0%, 4.55% and 32.37%, respectively, according to mass loss of steel reinforcement. Based on observations during static load test, the damage developed in the specimens could be classified into four different stages, namely, micro-cracking, first visible cracks, cracks distribution, as well as damage localization and yielding. Analysis of the AE data reveals distinguishable trends for RA value and average frequency (AF) registered for different corrosion levels, respectively. Moreover, the index of damage (ID) derived from the AE energy parameters obtained during the first stage of damage was found to be useful as an indicator for evaluating the extent of corrosion damage of RC beam specimens at initial loadings. In addition, to provide a practical application of AE toward life span estimation of corroded beam specimen, a Weibull damage function was introduced to estimate the remaining flexural capacity of the beam specimens. Based on analysis as well, it is noted that tensile fracture became more dominant with an increase in corrosion level.

Dear Editor,

Hereby, it is my pleasure to submit to you our latest revised version of paper entitled "Monitoring Fracture of Steel Corroded Reinforced Concrete Members under Flexure by Acoustic Emission Technique" to be considered for publication in Journal of Construction and Building Materials in special issue (VSI ETNDT6).

Please accept our sincere thanks for the time and effort spent on reviewing our manuscript. Your comments were highly insightful and enabled us to greatly improve the quality of our manuscript. In the following pages are our responses to each of the comments of the reviewer as well as your own comments.

We hope that the revisions in the manuscript and our accompanying responses will be sufficient to make our manuscript suitable for publication in Construction Building and Materials. We shall look forward to hearing from you at your earliest convenience.

Thank you again for your kind review and consideration.

Best Regards,

Hwa Kian CHAI
School of Engineering
The University of Edinburgh
Edinburgh, Scotland.

Answers for Reviewers

Reviewers' comments:

The paper is well revised. One small remark: the fact that the RA value follows the inverse order of corrosion (low RA-high corrosion, high RA-low corrosion) should be more clearly mentioned in the conclusions as it is very innovative and shows that concrete with highly corroded reinforcement operate relatively more in tension, due to bad cohesion between steel and matrix. This is in accordance to conclusion 1 which states that the HC specimen exhibited less cracks.

Thank you for the comments Prof.
We have improved the conclusions accordingly.

HIGHLIGHTS

- Fracture of the corroded beam specimens using AE technique has been conducted
- Magnitude of RA value decrease with the increase of corrosion level
- Index of damage was higher when the corrosion level increased at early stage of damage
- Weibull damage function was introduced to estimate the remaining flexural capacity of the specimens
- Tensile fracture became more dominant with an increase in corrosion level

Monitoring Fracture of Steel Corroded Reinforced Concrete Members under Flexure by Acoustic Emission Technique

Ahmad Zaki[a,d], Hwa Kian Chai[a,b], Arash Behnia[c], Dimitrios G. Aggelis[e], Jun Ying Tan[a], Zainah Ibrahim[a]

[a] *Department of Civil Engineering, Faculty of Engineering, University of Malaya, 50603 Kuala Lumpur, Malaysia.*

[b] *School of Engineering, University of Edinburg, Edinburgh, EH9 3JL Scotland, United Kingdom*

[c] *Discipline of Civil Engineering, School of Engineering, Monash University, Sunway Campus, Malaysia*

[d] *Department of Civil Engineering, Faculty of Engineering, Universitas Abdurrab, 28291, Pekanbaru, Indonesia*

[e] *Department of Mechanics of Materials and Constructions, Vrije Universiteit Brussels, Pleinlaan 2, Brussels 1050, Belgium*

Abstract

Acoustic emission (AE) technique is used for monitoring and evaluating the influence of corrosion on the structural behaviour of steel reinforced concrete (RC) beams under three-point flexure test. In this study, steel corrosion was accelerated by electro-chemical method utilising a direct current (DC) power supply and 5% sodium chloride (NaCl) solution. The steel corrosion that was induced into beam specimens casting were estimated at 0%, 4.55% and 32.37%, respectively, according to mass loss of steel reinforcement. Based on observations during static load test, the damage developed in the specimens could be classified into four different stages, namely, micro-cracking, first visible cracks, cracks distribution, as well as damage localization and yielding. Analysis of the AE data reveals distinguishable trends for RA value and average frequency (AF) registered for different corrosion levels, respectively. Moreover, the index of damage (ID) derived from the AE energy parameters obtained during the first stage of damage was found to be useful as an

indicator for evaluating the extent of corrosion damage of RC beam specimens at initial loadings. In addition, to provide a practical application of AE toward life span estimation of corroded beam specimen, a Weibull damage function was introduced to estimate the remaining flexural capacity of the beam specimens. Based on analysis as well, it is noted that tensile fracture became more dominant with an increase in corrosion level.

***Keywords**: Acoustic emission; steel corrosion; Damage probability function; Reinforced concrete; Weibull distribution; Concrete fracture monitoring*

1. Introduction

Corrosion of steel reinforcements in reinforced concrete (RC) structures is a worldwide problem. The corrosion has been recognized as the major deterioration mechanism which affects RC degradation due to the environmental actions [1]. The costs of repair and maintenance of corroded structures worldwide exceed billions of dollars per year [2, 3]. Therefore, the effects of steel corrosion in RC structures must be evaluated at early stage detection using effective assessment method before the functionality of RC structures is seriously damaged [4].

Non-destructive testing (NDT) methods provide objective-oriented assessment to different kinds of damages in RC structures, e.g. crack, honeycomb and corrosion. For newly built structures, the principal application of an NDT method is on the quality control, while for structures already in service, the method is expected to provide the needed feedback in monitoring, detection and identification of damage [5, 6]. NDT methods are non-intrusive, highly repeatable and cost-effective in terms of the execution time and accessibility [7]. Recently, some NDT methods have been implemented for corrosion monitoring of RC structures. They can be classified into six main categories as follows: visual inspection, electrochemical methods (i.e. open circuit potential (OCP), resistivity method, polarization

resistance, galvanostatic pulse method (GPM) and electrochemical noise (EN)), elastic wave methods (i.e. ultrasonic pulse velocity (UPV), acoustic emission (AE) and impact echo (IE)), electromagnetic (EM) methods (i.e. ground penetrating radar (GPR)), optical sensing methods (i.e. fibre Bragg grating (FBG)) and infrared thermography (IRT) method [8]. Each of the NDT methods has been used for monitoring, evaluating and assessing of the steel corrosion in RC structures with mixed levels of success. Despite mixed levels of successes by the afore-mentioned methods, there is an increase demand for a reliable technique to be applied in-situ that helps evaluate the effect of steel reinforcement corrosion in RC structures from the structural engineering point of view.

The AE technique has also been used to detect steel corrosion in RC structures [9-11]. The elastic wave energies resulted from fracture of concrete matrix by steel corrosion activity can be successfully detected by AE sensors placed on the concrete surface. The use of AE technique also enables localization of corrosion damage in addition to detecting micro- and macro-cracking fractures [12-14]. To the authors' knowledge, the first recorded application of the AE technique for corrosion evaluation in RC structures was by Dunn et al. [15]. By comparing measured AE characteristics, namely counts and amplitude distributions, a relation between the observed damage and the AE was developed. The study illustrated the sensitivity of the AE to the ongoing deterioration process and explores its use as a corrosion damage monitoring technique. In some later studies, AE parameters such as accumulated hits, signal strength and energy were successfully used to identify and characterize the process of steel corrosion in RC structures [11, 16-19]. The AE sources were also classified in terms of RA value and average frequency (AF) to distinguish the type of failure. Besides, the *b*-value and *Ib*-value of AE amplitude distribution were also proposed for assessing the damage severity [18, 20-22]. However, limited studies have been attempted to evaluate the fracture behavior of corroded RC structures using the AE technique. Kawasaki et al. [10] have carried out the AE

technique during a flexure test in RC beam specimens which were corroded by wet and dry cycles. The authors have applied the AE technique to evaluate the seismic capacity of corroded beam specimens. Results showed that the amount of tensile crack was greater than shear crack in the beam specimens with relatively low chloride contents, and vice versa.

In this study, the AE technique is utilized to evaluate the fracture behaviour of corroded beam specimens subjected to static loading. The beam specimens were corroded by the impressed current technique. This technique is able to simulate high level of steel corrosion in concrete within a short time period with easy control on the desired level [3, 23]. In order to characterize the fracture of corroded beam specimens subjected to bending, the AE parameters, namely RA value and AF, index of damage (ID) and Weibull damage have been carried out. Furthermore, examination was also conducted on the trend of the monitored AE data for use in determining the corrosion level at early stage of the loading.

2. AE parameters for assessing steel corrosion in RC structures

The parameter-based analysis of AE signal is useful for better characterization of AE source [24-28]. Parametric analysis of the cumulative AE hits, rise time, average frequency (AF), signal strength, energy, *b*-value, *Ib*-value and intensity analysis (IA) are applicable in detecting and assessing the steel corrosion in RC structures. The early number of cumulative AE hits can detect the steel corrosion at early stage [11, 20]. The sudden rise in cumulative signal strength (CSS) [29] and absolute energy (ABS) [30] might indicate crack initiation due to steel corrosion. On the other hand, the distribution of RA value and AF also proposed as a means of classifying the onset of steel corrosion and nucleation of cracks in RC structures [20]. In addition, previous researches have indicated that a *b*-value below 1.0 indicates the transition from micro- to macro-cracking [31, 32]. The large fluctuations in *Ib*-value imply that these cracks are generally repeated due to expansion of corrosion products [20]. On the other hand,

IA uses several criteria to identify the condition in the RC structures (i.e. no corrosion, early corrosion and cracking) [29].

2.1. RA value and Average frequency (AF)

The characteristics of AE signals are estimated using two parameters, namely RA value and average frequency (AF) in line with the relevant recommendations [26]. The RA value and AF are defined from the AE parameters, i.e. rise time, peak amplitude, counts and duration [18, 19], as given by Equations (1) and (2).

$$\text{RA value} = \text{Rise Time/Peak Amplitude} \quad (1)$$

$$\text{Average frequency (AF)} = \text{Counts/Duration Time} \quad (2)$$

A crack type is classified by the relationship between RA value and AF as shown in Fig. 1. A tensile-type crack is referred to as an AE signal with high AF and low RA value. A shear-type crack is identified by low AF and high RA value. This criterion is also used to classify AE data detected from the steel corrosion in the RC structures [11, 20].

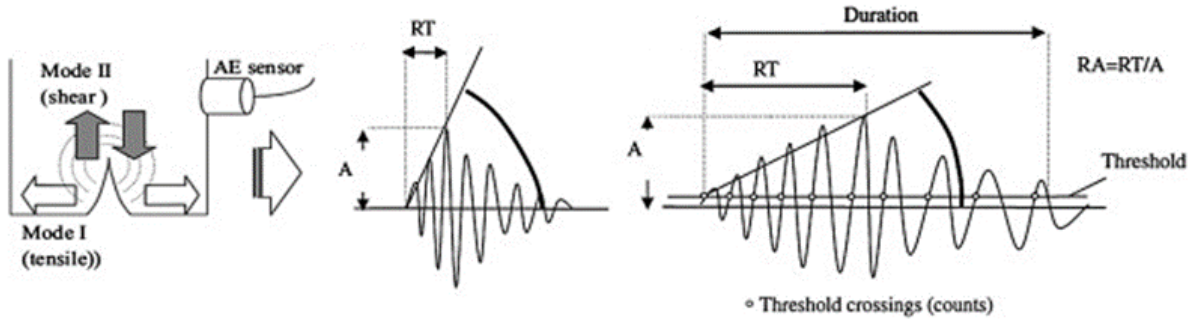

Fig. 1. (a) Classification of cracks by AE indices, (b) Tensile cracks and (c) Shear cracks [33].

2.2. Index of Damage (ID)

Benavent-Climent et al. [34, 35] have proposed a damage evaluation method based on accumulated AE energy with plastic strain energy as index of damage (ID). The authors developed this index during a seismic loading of RC slab using a uniaxial shake table to predict the level of damage based on the AE energy recorded by the AE sensors. On the other hand, Abdelrahman et al. [36] derived another method to obtain ID, which is based on dividing the cumulative AE energy at any instant of the test (E^{AE}) by the cumulative energy registered at the end of loading, in which specimen under investigation experienced the maximum allowable damage ($E_D{}^{AE}$). The ID can be expressed by Equation (3):

$$ID = E^{AE}/E_D{}^{AE} \quad (3)$$

2.3. Damage Statistical Model by Mesoscopic Element Probability Function

Reinforced concrete (RC) is a heterogeneous composite material that may be exposed to different types of deteriorations throughout the lifetime of usage, such as fracture, corrosion and surface degradation. The mechanical behaviour of deteriorated RC element with corrosion will become more complex because of stochastic distribution of damages. In addition, deterioration process in corroded RC element is localized and randomly distributed. Consequently, the strength of a corroded RC element can be regarded as a stochastic variable integrating different parameters, such as level of corrosion, location of corrosion, residual bond capacity, distribution of flaw, aggregate size and etc. Although the above mentioned parameters are independent to each other, this independency lies within certain mutual statistical rules. Accordingly, the damage and residual strength of the RC element can be expressed in statistical concept. Based on the statistical theory of damage for quasi-brittle materials, RC can be considered to be composed of many micro-elements. Although the rupture probability of each micro-element may be different under external load, the damage

probability of RC as a heterogeneous material is in compliance with a Weibull distribution [36]. The typical probability density function of a Weibull random can be expressed as below:

$$f\ (x;\lambda,k) = \frac{k}{\lambda}(\frac{x}{\lambda})^{k-1}\ e^{-(x/\lambda)^k} x \geq\ 0 \tag{4}$$

where, x is defined as a random variable, the shape parameter k is the Weibull modulus and λ is a scale parameter.

The following assumptions are made to utilize damage Weibull distribution on RC elements:

1. The stress-strain behaviour of each representative mesoscopic (volume) element was considered linear until it breaks;
2. At the time of mesoscopic element breaks, the load carried prior to failure will be transferred equally among the surviving mesoscopic elements;
3. The strength distribution of RC element can be represented by the well-known Weibull function as below:

$$D = 1\text{-}EXP\ (\frac{\varepsilon}{n})^m \tag{5}$$

where, m is defined as fractal dimension parameter, n is scale size parameter and ε is strain [37].

In addition, the rupture probability density function of the mesoscopic element could be described as follows [37]:

$$f\ (\varepsilon) =\ nm\ (\varepsilon - \varepsilon_0)^{m-1} \exp[-n(\varepsilon - \varepsilon_0)^m] \tag{6}$$

where, ε_0 is determined by experimental results and parameters of n and m are related to the dimensions and elastic properties of the RC specimens.

In probability theory, a probability density function (PDF) or density of a continuous random variable, is known as a function through which the relative likelihood for this random variable to take on a given value is explained. The probability of the random variable falling

within a particular range of values is given by the integral of this variable's density over that range. Consequently, the rupture probability up to the strain level ε will be obtained by integration of Equation (6), which is given by Equation (7).

$$F(\varepsilon) = \int f(\varepsilon) = \int nm\,(\varepsilon - \varepsilon_0)^{m-1} \exp\left[-n(\varepsilon - \varepsilon_0)^m\right] = 1 - \exp\left[-n(\varepsilon - \varepsilon_0)^m\right. \quad (7)$$

On the other hand, the ratio of $dN_\varepsilon/d\varepsilon$ to the total AE events N_{tot} can address the rupture probability density as given in the equation below:

$$f(\varepsilon) = (dN_\varepsilon/d\varepsilon)/N_{tot} \quad (8)$$

where, ε is strain/displacement in the beam and N_ε is defined as the sum of cumulated AE energy.

Subsequently, the Weibull damage function can be modified as below:

$$F(\varepsilon) = \int f(\varepsilon) = N_\varepsilon/Ntot \quad (9)$$

The bi-logarithmic regression analysis of the acquired AE data with respect to the ε was performed to obtain the n and m values for the RC element.

$$ln\left[-ln\left(1 - \frac{N_\varepsilon}{N_{tot}}\right)\right] = m\,ln(\varepsilon - \varepsilon_0) + ln\,n \quad (10)$$

The standard expression of linear regression with logarithm terms x and y is:

$$y = ax + b \quad (11)$$

where, y = $ln\left[-ln\left(1 - \frac{N_\varepsilon}{N_{tot}}\right)\right]$, x= $ln(\varepsilon - \varepsilon_0)$, $a = m$ and $b = ln\ n$ and ε_0 is defined as the deflection when the first AE signal is emitted and the AE measurements can determine the n and m parameters.

These parameters influence fracture resistance in the event of cracking. By adopting the aforementioned statistical models and performing integration, calibration for the Weibull damage function parameters can be done using AE data acquired from monitoring work.

3. Experimental Test

3.1. Materials and specimens preparation

Three beam specimens (i.e. 1000 x 150 x 150 mm^3) with details shown in Fig. 2 were prepared in the study. The beam specimen was designed in accordance to BS 8110-1 [38] to achieve 30 MPa of compressive strength at 28 days after casting. For reinforcements, deformed bars of sizes 12 mm and 16 mm complying to BS 4449 [39] were used as compression and tension bars, respectively. The stirrup of size 8 mm and spacing 240 mm was used for shear links. The cover concrete was designed as 36 mm. The copper wire was connected with steel reinforcement and positive pole of power supply as anode of accelerated corrosion process. The accelerated corrosion process will be explained in following section. Table 1 gives the proportions of raw materials used for the concrete mix.

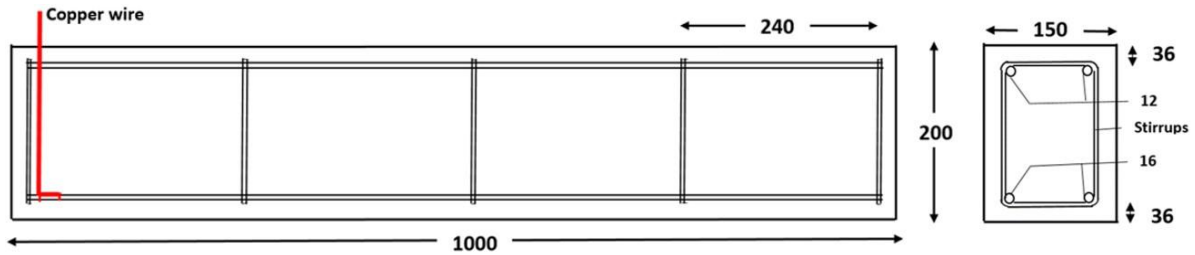

Fig. 2. Details of beam specimen (units are in mm)

Table 1
Mix proportions of beam specimen

w/c (%)	Weight of unit volume (kg/m^3)			Maximum aggregate size (mm)
	Cement	Fine Aggregate	Coarse Aggregate	
0.50	380	780	1080	20

where, w/c (%) = water cement ratio

3.2. Accelerated steel corrosion process

Among the three beam specimens, one was used as the Control beam specimen with no steel corrosion being induced. The other two beam specimens (i.e. Low Corrosion (LC) and High Corrosion (HC)) were simulated with steel corrosion generated at different levels 28 days after casting. The accelerated corrosion process adopted the impressed current technique that conforms to ASTM G1-03 [40] and ASTM G31-72 [41]. Fig. 3 shows the set-up of the accelerated corrosion process. The specimen was partially immersed in 5% sodium chloride (NaCl) solution by volume in a plastic water tank. A direct current (DC) power supply was used in the electrolysis of the chemical solution, from which the positive terminal was connected by the copper wire to the steel reinforcement as the anode. Meanwhile, the negative terminal was connected by an aluminium plate as the cathode. A constant current of 1A was applied in the corrosion process. The durations of the corrosion process were 3 and 23 days to result in corrosion levels of 4.55 and 32.37 % by steel mass loss, respectively based on converting the current flow by Faraday's law to metal loss using the following equation:

$$\Delta m = \frac{M.I.t}{z.F} \tag{12}$$

where, Δm is mass of steel consumed (g, gram), M is atomic or molecular weight of metal (56 g/mol for steel), I is current (A, amperes), t is time current or potentials applied (s, seconds), z is ionic charge or electrons transferred in the half-cell reaction (2 for steel) and F is Faraday's constant (96500 A/s).

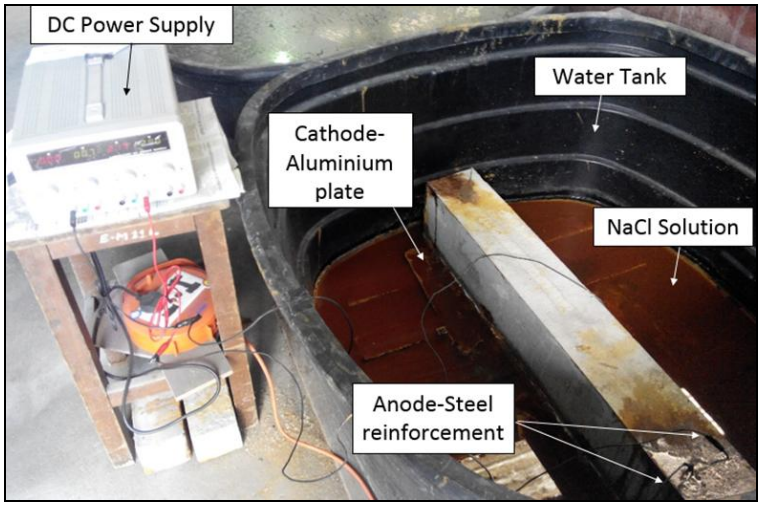

Fig. 3. Experimental setup of the accelerated corrosion process

After the flexure tests, the beam specimens were hacked to retrieve the steel reinforcements. The steel reinforcements were then cleaned to remove rust in accordance to ASTM G1-2003 [40] and weighed to determine the actual mass loss of steel reinforcement.

3.3. Load testing and AE system

All the beam specimens were subjected to three-point monotonic flexural load using a universal testing machine (INSTRON Satec Series) with a maximum capacity of 600 kN. AE monitoring of beam fracture was conducted throughout the loading test. For this, a six-channel PCI-2 AE System (MITRAS Group, Inc.) were used. The system was connected by six AE sensors of 150 kHz resonant frequency (SR150N) together with 40 dB preamplifiers by Soundwel Co., Ltd. The sensors were mounted to surface of concrete using electron wax as the coupling agent. Fig. 4 illustrates the sensor placements on beam specimen. In the measurements, the sampling rate was set to 2 MHz, with pre-trigger at 256.000 μs and data length at 2k. The hit definition time and hit lockout time were configured as 800 μs and 1000 μs, respectively. To eliminate electrical and mechanical noises generated during monitoring, the threshold level was set at 45 dB.

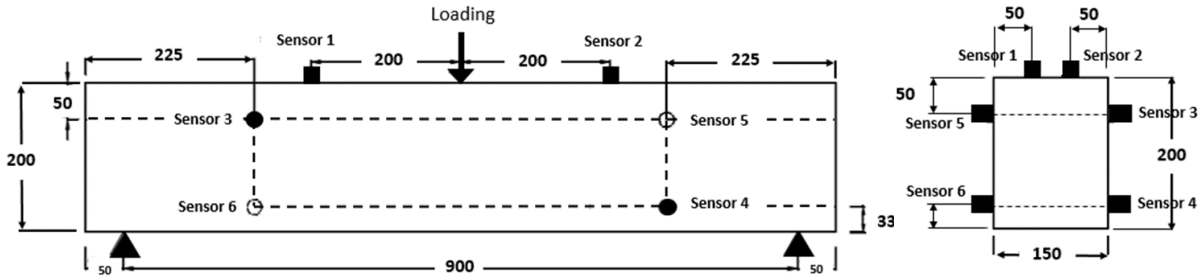

Fig. 4. AE sensor placements on beam specimen (units are in mm)

4. Results and Discussion

4.1. Mechanical Behaviour

Fig. 5 shows the load against mid-span deflection curves of the beam specimens. The failure load dropped from approximately 182 kN for the Control beam specimen to less than 150 kN for LC and HC beam specimens, justifying the decrease in beam stiffness as a result of steel corrosion. It is also found that the two corroded beam specimens did not registered significant difference between their failure loads, which were approximately 145 kN and 148 kN, respectively. The LC and HC beam specimens show exhibited nearly similar behavior in terms of ductility which was higher than the Control beam specimen.

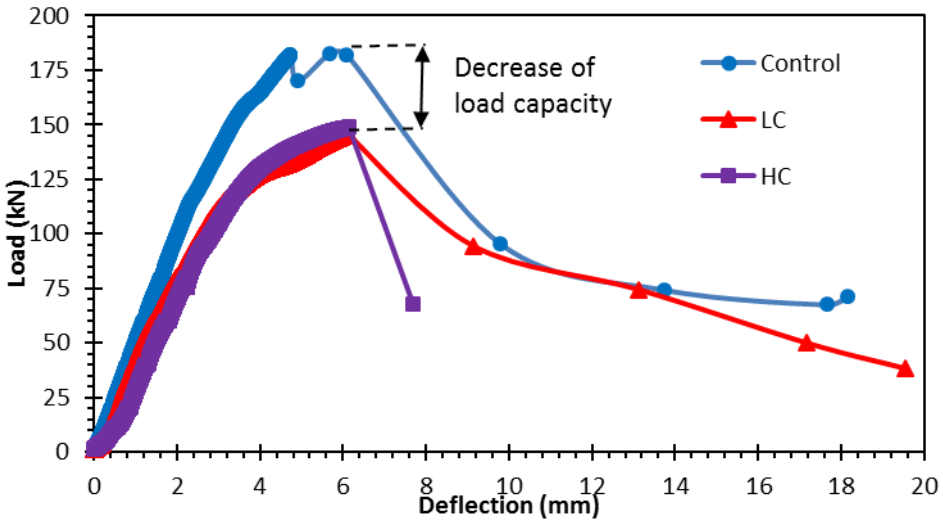

Fig. 5. Load versus mid-span deflection of the beam specimens

The condition of beam fracture at the end of loading test is shown in Fig. 6. From observations during testing, all the three beam specimens were found to fail by developing macroscopic fracture in shear, signified by the formation of diagonal crack that eventually penetrated through the specimen height. At the initial stage of loading, the first visible crack was observed from the concrete side face of all the three beam specimens, which propagated from bottom of the specimen between loads of 47 kN to 55 kN. As the load increased, more cracks were found propagating vertically from bottom of the beam specimen to indicate tensile fracture under flexure. Diagonal cracks were also found initiated from concrete above the supports and progressed towards the location where the load was applied, at 95 kN, 87 kN and 100 kN for the Control, LC and HC beam specimens, respectively. Continuous increase in the load resulted in the start of steel reinforcement yielding and beam fracture localization to form macro-cracks, at 120 kN, 137 kN and 134 kN for the Control, LC and HC beam specimens, respectively.

For the Control beam specimen, the amount of visible cracks observed until failure occurred was found to be more than the two corroded beam specimens. Rust stain was evident from the side face of HC beam specimen at proximity of tension reinforcements, where horizontal cracks were also seen. This indicated fracture of the beam specimen by formation of expansive corrosion product on tensile steel reinforcements. This has resulted in decrease of bond strength between steel reinforcement and beam specimen, affecting stress distribution within the beam specimen when flexural load was applied. The doweling action was noticeable during the loading, with which splitting of concrete cover occurred by macroscopic cracking along the steel reinforcements from beam end. The crack was then directed diagonally upwards to the point of loading to form brittle shear failure, which occurrence was similar to that observed for the Control beam specimen.

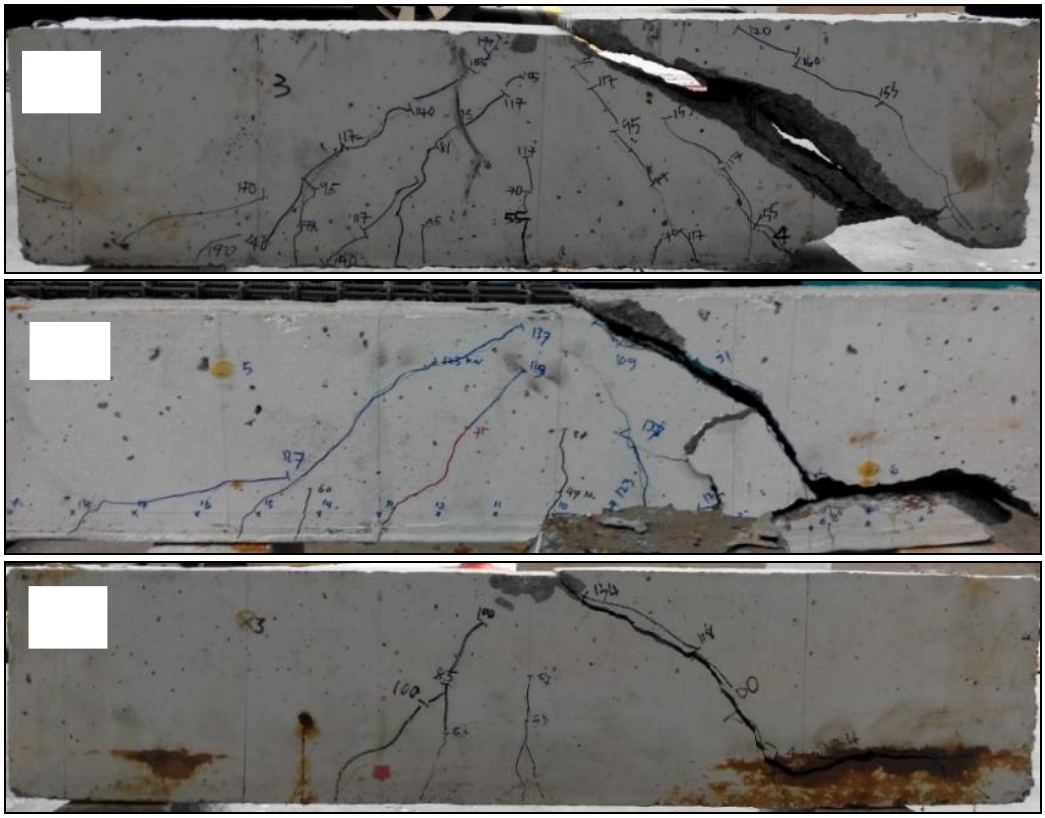

Fig. 6. Cracking as observed at failure for (a) Control, (b) LC and (c) HC beam specimens

In general, the fracture of beam specimens can be classified into four damage stages as shown in Fig. 7, which were suggested by some previous study on flexural behavior of RC structures. The damage stage can help to characterize the concrete behaviour in relationship between load and deflection with the AE parameters. Analyzing AE data at each stage of damage can help to overcome the overlap among stages and to classify the crack types [37, 38]. Although the first visible crack was found at approximately 30-35 % of the ultimate load. Prior to this, micro-cracking was considered to have taken place within the beam specimens, whose occurrence could be detected with the AE monitoring. It was also observed that the location of the first visible crack was near to the mid-span of the beam specimens. Damage Stage III, known as the crack distribution stage, was detected when load reached approximately 50% of its ultimate load. This process was observed till the flexural moment

reached damage Stage IV, with steel reinforcement damage localization and yielding started at approximately 81-86 % of the ultimate load, micro-cracking should have when loading commenced and cracks distributed and coalesced to give localized macroscopic fracture. By considering the definition of stiffness, Fig. 7 shows that as the load increases the slope of load-deflection curve decreased which implies that the stiffness of the beam specimens decrease with the widening of the cracks at mid-span. Apparently, Control beam specimen has more brittle characteristics than the other two beam specimens (i.e. LC and HC).

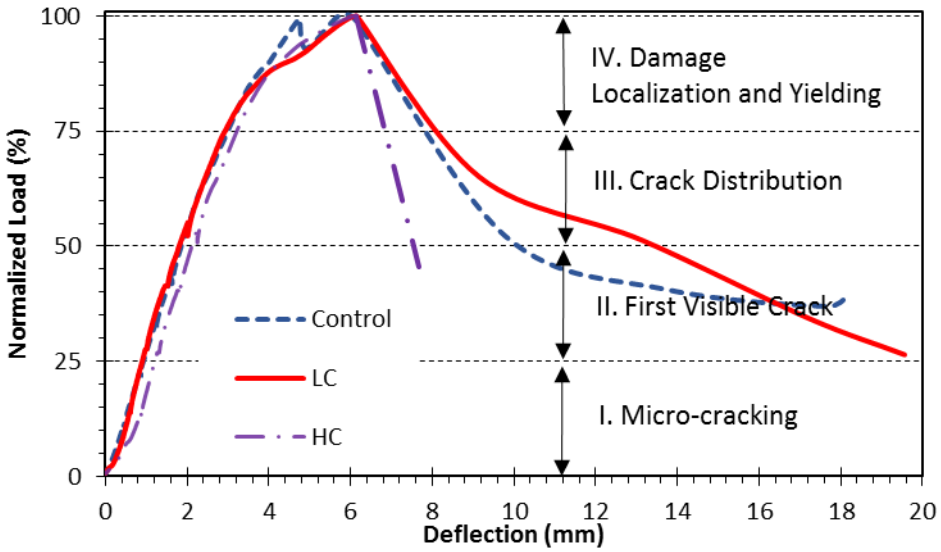

Fig. 7. Damage stage classification of the beam specimens

4.2. Characteristics of AE parameters

4.2.1. Crack classifications – RA value and AF

The change in RA value and AF is used to evaluate the mode of fracture in the beam specimens. The two AE parameters can be computed using Equations (1) and (2). Previous findings suggested that in tensile mode cracking, AE rise time would be shorter, with higher average frequency but lower RA value as compared with those registered for shear mode cracking [33]. The variations are mainly attributed to the change in the transmitted energy and its speed, which were correlated in an inversed manner. Hence, the energy speed at the

later stages of damage is always slower than that at the earlier stages because of the larger part of energy being transferred in shear waves form [42].

Fig. 8 gives the plots of RA value and AF against time, computed from the monitored AE data in the current study, by averaging the respective values at every 5% load increment. It can be seen from the plots that in general, after the first load level (5% of ultimate load), the RA value experienced a decrease and AF abruptly increased before gradually rose back in subsequent load levels. From the relationship, tensile cracks were observed from the beginning of the load. For the Control beam specimen, the RA value and AF register steady increase after not long after load was applied, as recorded from the middle of damage Stage I (10% of ultimate load) to the early stage of damage Stage IV (80% of ultimate load), during which micro-fracture in tensile crack mode were observed to propagate extensively and coalesced, at the same time shear cracking started to initiate. On the other hand, the RA value and AF of LC beam specimen gradually increased from the end of damage Stage I (20% of ultimate load). Starting from damage Stage III (50% of ultimate load), the RA value dropped, in contrast to marked increase in AF to imply the occurrence of beam rupture by cracking and steel corrosion activities [33]. The crack mode was classified as the tensile cracks at the bond of tension reinforcements in the beam specimen.

The highest recorded RA value is obtained from the last damage stage of the Control and LC beam specimens, as shown in Figs. 8 (a) and (b). This indicates a trend for shear crack development and progression due to ultimate fracture. However, for the HC beam specimen, the highest RA value and the decrease AF occurred towards the end of the damage Stage II, which, at this condition, the shear cracks have been observed to start propagating from the tension side of the beam specimen, at the proximity of the steel reinforcements. After reaching the peak, the RA value marked a sharp decrease before gradually increases from the damage Stage III. There is a relatively large increase in RA value at the start of

damage Stage IV, but the magnitude is lower than that obtained earlier. This implies that the most corrosion-induced cracks were progressed further and nucleated at the end of damage Stage II, compared with the damage Stage IV. According to the RA value and AF of the AE parameters, the effect of increase corrosion level of the beam specimens was confirmed by the lower magnitude of RA value. In the HC beam specimen, the magnitude of RA value was lowest and nucleated at an earlier stage than Control and LC beam specimens.

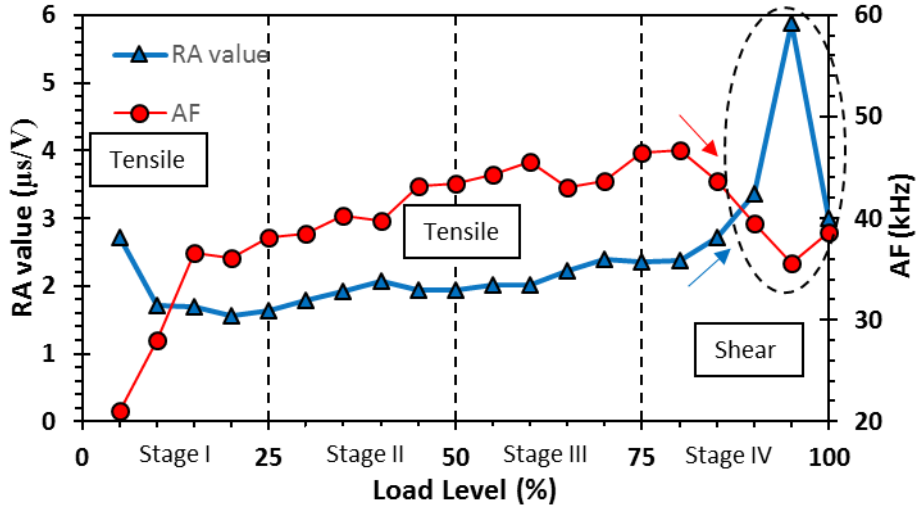

(a)

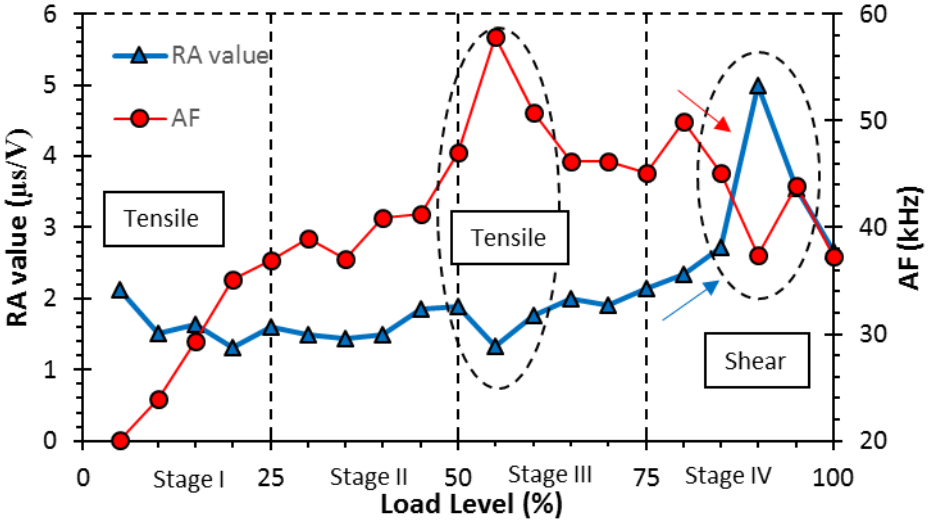

(b)

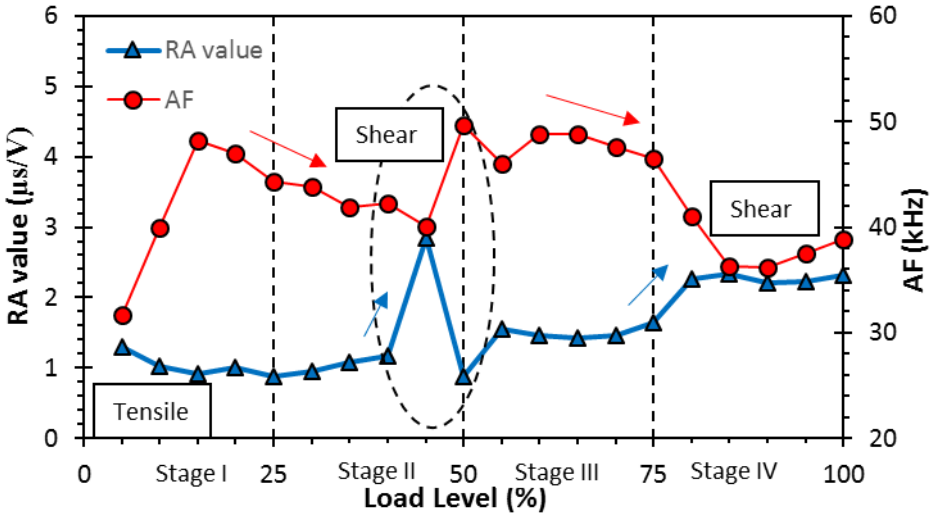

(c)

Fig. 8. Variation of RA value and AF with load for (a) Control, (b) LC and (c) HC beam specimens

The average RA value was calculated for each stage of damage for all the beam specimens with reference to the work reported by Aldahdooh et al. [42]. From Fig. 9 that shows the results of computation, the average RA value increased with the development of damage for all the beam specimens. In damage Stage I, the average RA value decreased with the increase of the corrosion level. This stage was associated with the initial or micro-cracking until the formation of the first visible crack. The feasible interpretation of this result was related with the mechanical behaviour of the beam specimens, as the corrosion level increased for a given load, the number of tensile cracks decreased. Because of that, the RA value tend to decrease and the AF is high. The average RA value acquired from this damage stage is useful as an early indicator to the imminent formation of visible cracking due to the deterioration by steel corrosion activity. In overall, the average RA value is also lower for higher corrosion level, however, when the shear cracks initiated, the RA value increased evidently as shown in damage Stage IV.

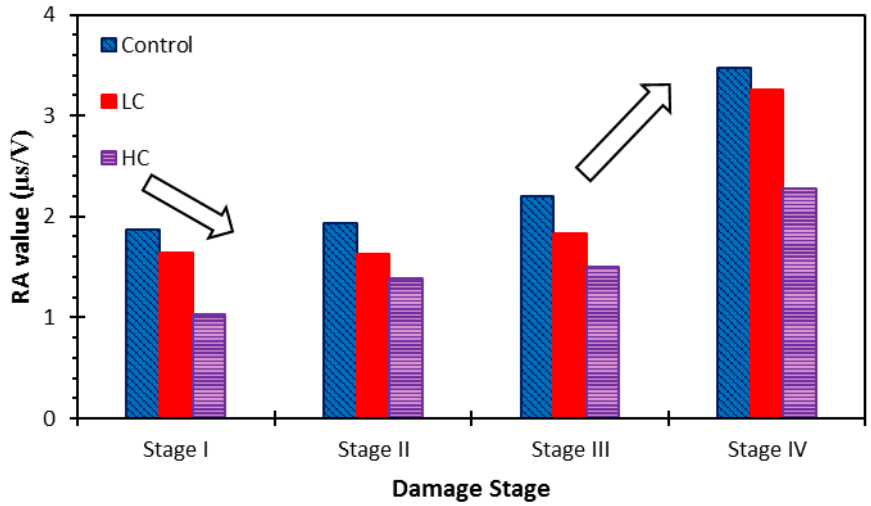

Fig. 9. Average RA value at each load stage of the beam specimens

Fig. 10 shows RA value againts AF distribution of the AE data per 5% of ultimate load. It is shown that as the corrosion level becomes higher (from Control to LC and HC beam specimens), there is a collective increase in AF and a decrease in RA value of the beam specimens. On the other hand, it also indicates the transition of the beam specimen dominating fracture behaviour, which shifts from tensile to shear as the damage stage increases (from damage Stage I to IV) in accordance to the classification method suggested previously [10, 27, 35].

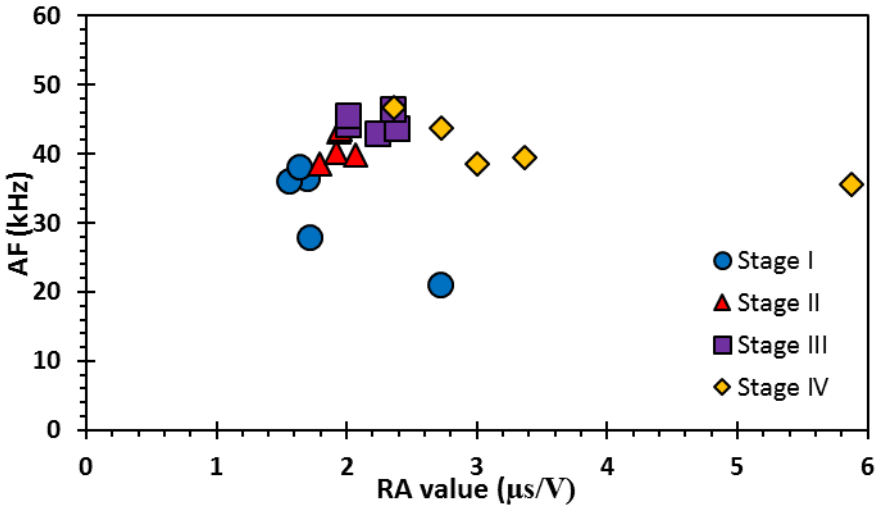

(a)

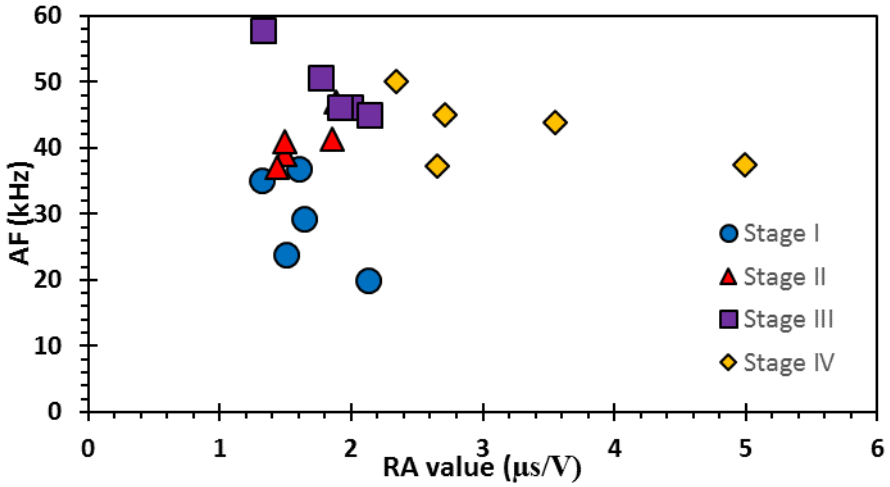

(b)

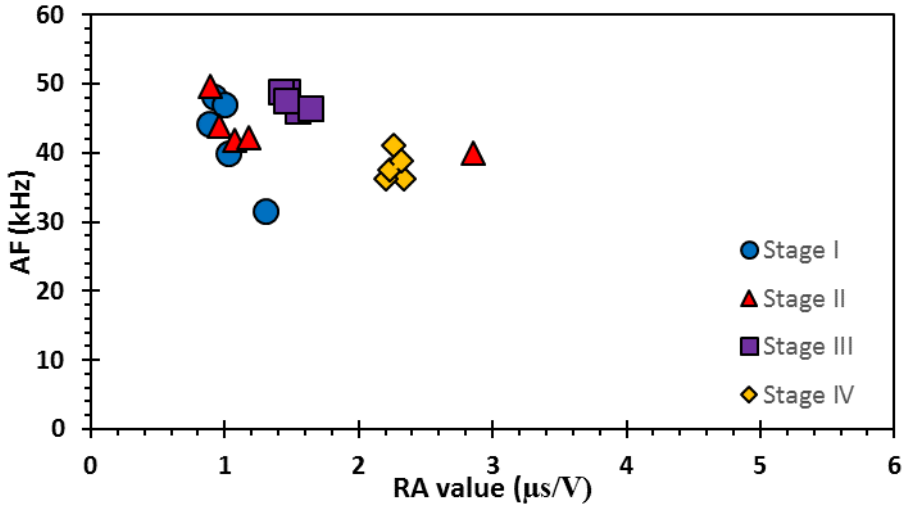

(c)

Fig. 10. RA value versus AF for (a) Control, (b) LC and (c) HC beam specimens

4.2.2. Damage evaluation - Index of Damage

Table 2 shows the total AE energy recorded in all the damage stages of the beam specimens. From the table, the total AE energy recorded for the HC beam specimen was the lowest among the three. On the other hand, the total AE energy increased with progression of the damage stage. The total AE energy was the highest for damage Stage IV, indicating that macroscopic fractures have taken place [27]. However, for the HC beam specimen, the total AE energy damage for damage Stages II and III were comparable. In addition, the total AE energy obtained for damage Stage IV of the specimen was significantly lower than the other

two beam specimens. These findings implied that the formation of new cracks in the HC beam specimen was relatively fewer than the other two beam specimens and majority of the cracking could have occurred during the steel corrosion process that was not monitored by AE.

Table 2.
Total AE energy for each damage stage

Specimen	Stage I	Stage II	Stage III	Stage IV	Total
Control	697,205	2,949,516	7,243,477	16,442,895	**27,333,093**
LC	979,874	2,987,582	5,061,069	34,539,102	**43,567,627**
HC	899,470	5,858,081	5,086,416	7,271,464	**19,115,431**

The ID from each damage stage is given in Fig. 11. The suggested index was calculated by dividing the cumulative AE energy obtained from the respective load levels (percentage of instantaneous load in relative to failure load) with those acquired at ultimate failure. At damage Stage I, the ID is higher when the corrosion level of the beam specimen increased, as shown in Fig. 11(b). However, the ID of LC beam specimen is slightly higher than that of HC beam specimen. These result was probably due to the effect of steel corrosion of LC beam specimen to the structural performance of the beam specimen higher than HC beam specimen. The AE energy measured from this damage stage was closely associated with the actual condition of corroded beam specimens before the occurrence of visible cracking to signify the initiation of permanent damage. From damage Stage II to III, the ID for the HC beam specimen increased and became the highest among three beam specimens. An explicit pattern for the development of ID was found, which can be described as a sudden change in slope of the data line that could be related to the occurrence of fractures, especially the ones that occurred at the interface between concrete and steel reinforcements. The

fracture was considered to be dominant in damage Stages II and III. In damage Stage IV, after yielding point, the increase in the data slope could be clearly pointed for the Control and LC beam specimens, manifesting relatively high AE activities that were generated from the extensive cracking and fracturing towards the ultimate failure of the beam specimens.

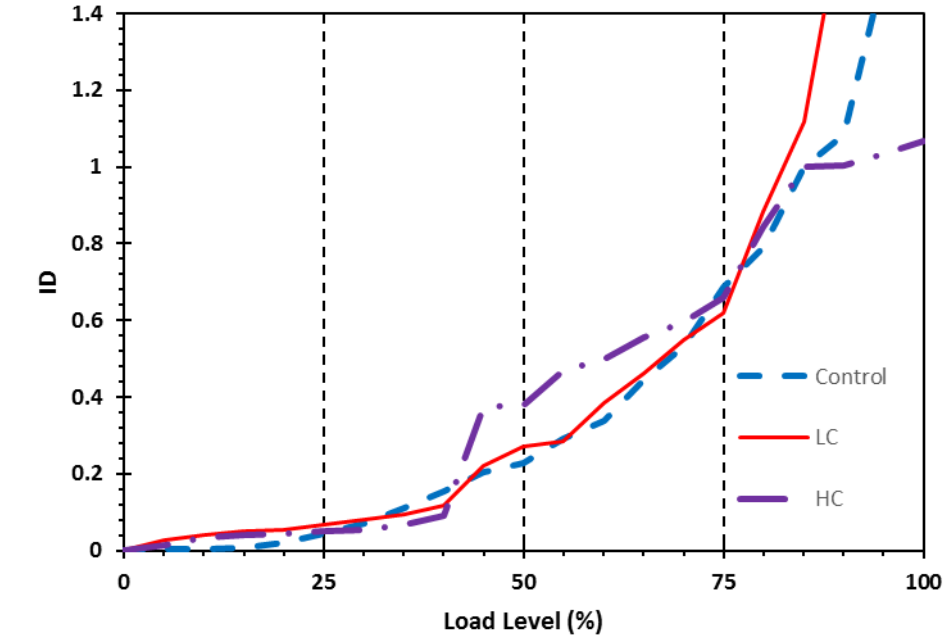

(a)

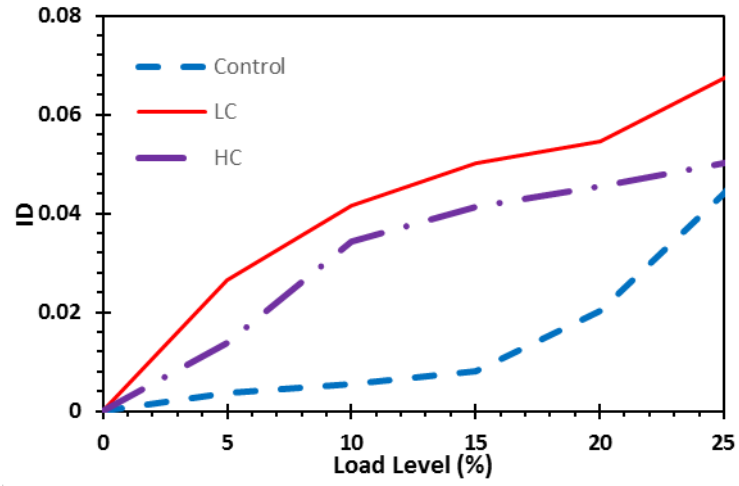

(b)

Fig. 11. ID distributions at (a) each load level (%) and (b) damage Stage I

4.2.3. Damage Statistical Model by Mesoscopic Element Probability Function

As observed, the AE total energy could provide ID pertaining to each load level. However, the need for total AE energy and reproduction of AE data is a drawback for practical application of this index in real structures. Therefore, a damage statistical model was developed to overcome the above mentioned drawback using AE energy data as variable. Fig. 12 (a) shows the computed Weibull damage function and AE energy versus displacement for the Control beam specimen. A fitted trend line which used to facilitate regression is also shown in the logarithmic chart as in Fig. 12 (b).

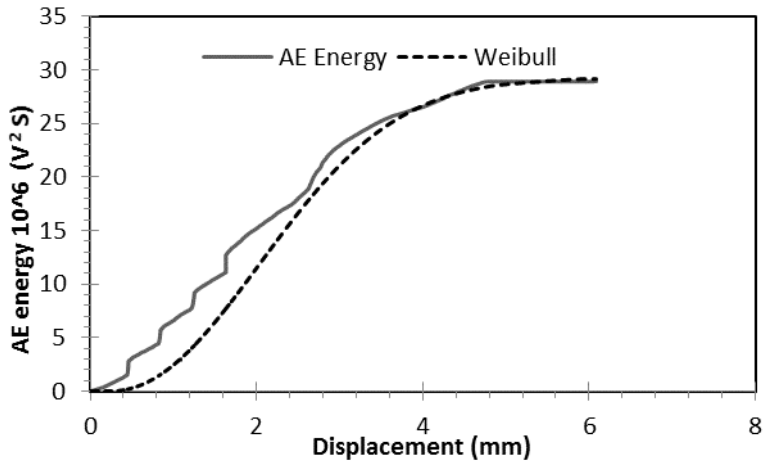

(a)

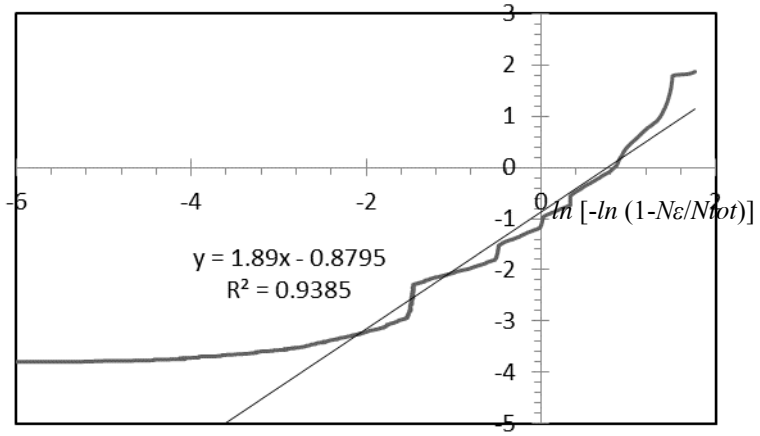

ln (ε-ε_0).

(b)

Fig. 12. (a) Weibull damage distribution and AE energy versus displacement and

(b)Weibull function calibration for Control beam specimen

The parameters *m*, *n*, R^2 and ε_0 were calibrated as 1.89, 0.41, 0.9385 and 0.0366, respectively. The obtained Weibull damage parameters were used to estimate AE energy to verify the accuracy and efficiency of proposed model. As depicted in Fig. 12 (a), the average absolute relative difference between cumulative AE energy and Weibull distribution curve is about 2.443% which is fairly acceptable. Therefore, the Weibull parameters were calibrated for the other two corroded beam specimens so that the damage probability function could be obtained for all beam specimens. The calibrated Weibull parameters by AE energy data are presented in Table 3.

Table 3
Parameters for Weibull damage functions

Specimen	m	n	R^2	Error %
Control	1.89	0.41	0.9385	6.15
LC	1.69	0.4	0.9249	7.51
HC	1.53	0.41	0.9136	8.64

Table 3 shows the calibrated Weibull parameters obtained by AE energy data, which is the reflection of mechanical performance of the beam specimens. It can be seen that the variation in *n* among the three beam specimens is negligible, probably due to the dimensions or size of beam specimens as *n* is related to size scale. On the contrary, it was obvious that the *m* changes in accordance to any change imposed to material properties and strength. It can be said that the change of *m* value was governed by fractal properties. In other words, higher value of *m* suggests higher strength of material. This has been reflected by the plots given in Figs. 13 (a) and (b) where damage probability of all the beam specimens, computed using cumulative AE energy data, is plotted against displacement and load. These figures show that the probablity of failure occurrence is higher for HC beam specimen at a lower load level compared to the other two beam specimens.

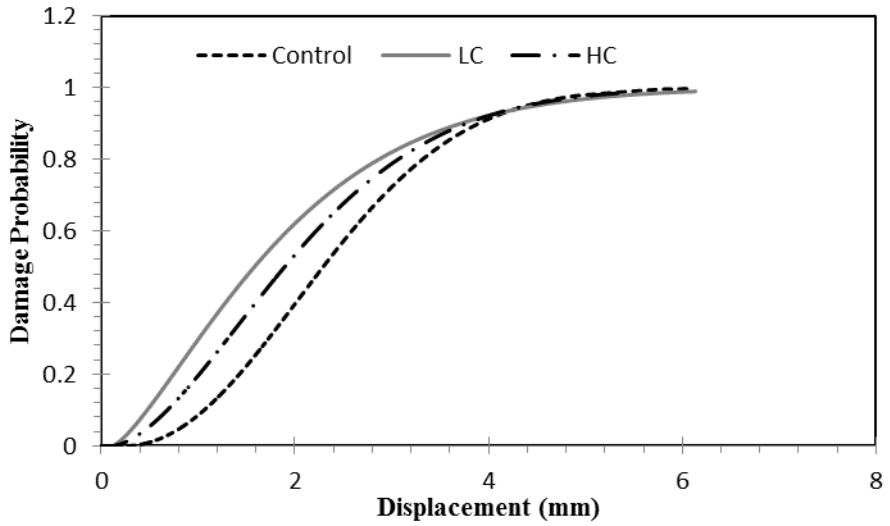

(a)

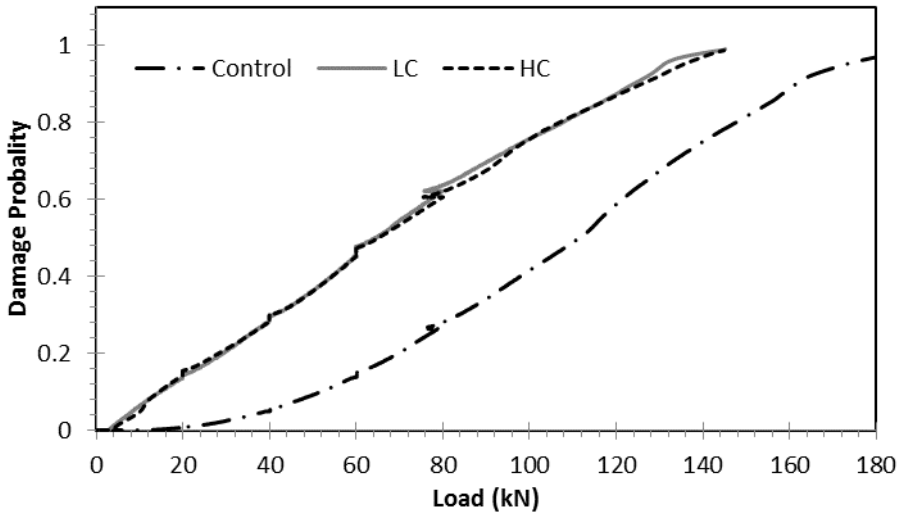

(b)

Fig. 13. (a) Damage probability function versus (a) displacement and (b) load of all beam specimens load

With successful utilization of AE energy data to define Weibull damage function for characterizing mechanical performance of the corroded beam specimens it is deduced that certain statistical relationships between material behavioural change and AE parameters may provide useful mechanical characterization of a structure from the early stage of fracture occurrence. The findings also provide insights to using AE monitoring technique in predicting the structural behaviour of steel corroded beam specimens under service load.

More studies will be required to further examine the reliability of this statistical approach and the feasibility of using other AE parameters.

5. Conclusions

In this study, the evaluation of the fracture behaviour of the corroded beam specimens under static loading using the AE technique has been successfully conducted. The conclusions drawn from this study can be summarised as follows:

1. Based on observations, all of the beam specimens failed in shear failure. The amount of cracks formed by the Control beam specimen was highest among all three beam specimens. The highly corroded beam specimens failed with fewer number of cracks, due to the deteriorated bond of steel reinforcements could not transfer the stresses to the concrete matrix.
2. For characterizing the beam behaviour in the relationship between load and deflection with the AE parameters, the development of the beam damage were defined into four damage stages (i.e. micro-cracks, first visible cracks, crack distribution, as well as damage localization and yielding). The RA value and AF of the AE parameters were used to evaluate the fracture mode in the beam specimens. The highest recorded RA value was obtained from the last damage stage, as shown in the Control and LC beam specimens. However, for the HC beam specimen, the highest RA value occurred at the end of the damage Stage II, which at this stage the shear cracks were observed to start propagating from the tension side of the beam specimen. On the other hand, the magnitude of RA value decrease with the increase of corrosion level. The magnitude of RA value obtained from beam specimen with the highest steel corrosion level, i.e. HC beam specimen was the lowest among the three beam specimens. The same beam specimen was also found to have operated more pronouncedly in tension, most probably

a result of deteriorated cohesion between steel reinforcements and concrete that affected transfer of stresses.

3. Based on the average RA value of the AE parameter that was calculated for each damage stage, it was confirmed that the average RA value increased with the development of the damage stage. On the other hand, at the damage Stage I, the decrease of average RA value with the increase of corrosion level was useful as an early indicator to the imminent formation of visible cracking due to steel corrosion of the beam specimens.
4. The damage evaluation of the corroded beam specimens based on ID was proposed. At the damage Stage I, the ID was higher when the corrosion level increased. The ID measured of this damage stage was closely associated with the condition of the corroded beam specimens before the occurrence of visible cracking to signify the initiation of permanent damage in the beam specimens.
5. The Weibull fracture parameters were calibrated by using AE energy data so that the failure probability function was successfully computed through which the remaining flexural capacity of the beam specimens was estimated.

Acknowledgments

This work was supported by the Minister of Higher Education (Malaysia) by providing the financial support for this project under Grant No. UM.C/625/1/HIR/MOHE/ENG/54. This work was also supported by the Postgraduate Research Fund (PPP), University of Malaya under Grant No. PG164-2015A.

References

[1] B. Elsener, C. Andrade, J. Gulikers, R. Polder, M. Raupach. Half-cell potential measurements - Potential mapping on reinforced concrete structures. Mater. Struct. 2003;36(7):461-471.
[2] S. Ahmad. Reinforcement corrosion in concrete structures, its monitoring and service life prediction - A review. Cem. Concr. Compos. 2003;25(4–5):459-471.
[3] Y. Yuan, Y. Ji, S.P. Shah. Comparison of two accelerated corrosion techniques for concrete structures. ACI Struct. J. 2007;104(3):344-347.
[4] J. Hugenschmidt, R. Mastrangelo. GPR inspection of concrete bridges. Cem. Concr. Compos. 2006;28(4):384-392.
[5] O. Büyüköztürk. Imaging of concrete structures. NDT and E Int. 1998;31(4):233-243.
[6] S.K.U. Rehman, Z. Ibrahim, S.A. Memon, M. Jameel. Nondestructive test methods for concrete bridges: A review. Constr. Build. Mater. 2016;107:58-86.
[7] S. Momoki, T. Shiotani, H.K. Chai, D.G. Aggelis, Y. Kobayashi. Large-scale evaluation of concrete repair by three-dimensional elastic-wave-based visualization technique. Struct. Health Monit. 2013;12(3):240-251.
[8] A. Zaki, H.K. Chai, D.G. Aggelis, N. Alver. Non-destructive evaluation for corrosion monitoring in concrete: A review and capability of acoustic emission technique. Sensors. 2015;15(8):19069-19101.
[9] H. Idrissi, A. Limam. Study and characterization by acoustic emission and electrochemical measurements of concrete deterioration caused by reinforcement steel corrosion. NDT and E Int. 2003;36(8):563-569.
[10] Y. Kawasaki, S. Wasada, T. Okamoto, K. Izuno. Evaluation for RC specimen damaged from rebar corrosion by acoustic emission technique. Constr. Build. Mater. 2014;67, Part B:157-164.
[11] Y. Kawasaki, Y. Tomoda, M. Ohtsu. AE monitoring of corrosion process in cyclic wet–dry test. Constr. Build. Mater. 2010;24(12):2353-2357.
[12] V. Leelalerkiet, T. Shimizu, Y. Tomoda, M. Ohtsu. Estimation of corrosion in reinforced concrete by electrochemical techniques and acoustic emission. J. Adv. Concr. Tech. 2005;3(1):137-147.
[13] D.G. Aggelis, D.V. Soulioti, N. Sapouridis, N.M. Barkoula, A.S. Paipetis, T.E. Matikas. Acoustic emission characterization of the fracture process in fibre reinforced concrete. Constr. Build. Mater. 2011;25(11):4126-4131.
[14] A. Behnia, H.K. Chai, M. Yorikawa, S. Momoki, M. Terazawa, T. Shiotani. Integrated non-destructive assessment of concrete structures under flexure by acoustic emission and travel time tomography. Constr. Build. Mater. 2014(0).
[15] S.E. Dunn, J.D. Young, W.H. Hartt, R.P. Brown. Acoustic emission characterization of corrosion induced damage in reinforced concrete. Corrosion. 1984;40(7):339-343.
[16] D.J. Yoon, W.J. Weiss, S.P. Shah. Assessing damage in corroded reinforced concrete using acoustic emission. J. Eng. Mech. 2000;126(3):273-283.
[17] M. Ohtsu, Y. Tomoda. Acoustic emission techniques for rebar corrosion in reinforced concrete. in: Advances in Construction Materials. 2007. pp. 615-621.
[18] M. Ohtsu, Y. Tomoda. Corrosion process in reinforced concrete Identified by acoustic emission. Mater. Trans. 2007;48(6):1184-1189.
[19] M. Ohtsu, Y. Tomoda. Phenomenological model of corrosion process in reinforced concrete identified by acoustic emission. ACI Mater. J. 2008;105(2):194-199.
[20] Y. Kawasaki, T. Wakuda, T. Kobarai, M. Ohtsu. Corrosion mechanisms in reinforced concrete by acoustic emission. Constr. Build. Mater. 2013;48(0):1240-1247.
[21] A. Behnia, H.K. Chai, T. Shiotani. Advanced structural health monitoring of concrete structures with the aid of acoustic emission. Constr. Build. Mater. 2014;65:282-302.
[22] M.K. ElBatanouny, P.H. Ziehl, A. Larosche, J. Mangual, F. Matta, A. Nanni. Acoustic emission monitoring for assessment of prestressed concrete beams. Constr. Build. Mater. 2014;58:46-53.
[23] Y. Yuan, Y. Ji. Modeling corroded section configuration of steel bar in concrete structure. Constr. Build. Mater. 2009;23(6):2461-2466.

[24] T.N.K. Titus, D.V. Reddy, S.E. Dunn, W.H. Hartt. Acoustic emission crack monitoring and prediction of remaining life of corroding reinforced concrete beams. in: 4th European Conference Non-destructive Testing. London, UK. 1988. pp. 1031-1040.
[25] M. Ohtsu. The history and development of acoustic emission in concrete engineering. Mag. Concr. Res. 1996;48(177):321-330.
[26] M. Ohtsu. Recommendation of RILEM TC 212-ACD: acoustic emission and related NDE techniques for crack detection and damage evaluation in concrete. Mater. Struct. 2010;43(9):1187-1189.
[27] A. Gallego, A. Benavent-Climent, E. Suarez. Concrete-galvanized steel pull-out bond assessed by acoustic emission. J. Mater. Civ. Eng. 2015;28(2).
[28] M.E. Zitto, R. Piotrkowski, A. Gallego, F. Sagasta, A. Benavent-Climent. Damage assessed by wavelet scale bands and b-value in dynamical tests of a reinforced concrete slab monitored with acoustic emission. Mech. Syst. Sig. Proc. 2015;60-61:75-89.
[29] W. Velez, F. Matta, P. Ziehl. Acoustic emission intensity analysis of corrosion in prestressed concrete piles. in: AIP Conference Proceedings. 2014. pp. 888-894.
[30] M. Ing, S. Austin, R. Lyons. Cover zone properties influencing acoustic emission due to corrosion. Cem. Concr. Res. 2005;35(2):284-295.
[31] M.K. ElBatanouny, A. Larosche, P. Mazzoleni, P.H. Ziehl, F. Matta, E. Zappa. Identification of cracking mechanisms in scaled FRP reinforced concrete beams using acoustic emission. Exp. Mech. 2012.
[32] K. Ono. Application of acoustic emission for structure diagnosis. Konferencja Naukowa. 2010:317-341.
[33] D.G. Aggelis. Classification of cracking mode in concrete by acoustic emission parameters. Mech. Res. Commun. 2011;38(3):153-157.
[34] A. Benavent-Climent, A. Gallego, J.M. Vico. An acoustic emission energy index for damage evaluation of reinforced concrete slabs under seismic loads. Struct. Health Monit. 2012;11(1):69-81.
[35] F. Sagasta, A. Benavent-Climent, A. Roldán, A. Gallego. Correlation of Plastic Strain Energy and Acoustic Emission Energy in Reinforced Concrete Structures. Appl. Sci. 2016;6(3).
[36] M. Abdelrahman, M.K. ElBatanouny, P.H. Ziehl. Acoustic emission based damage assessment method for prestressed concrete structures: Modified index of damage. Eng. Struct. 2014;60:258-264.
[37] A. Behnia, H.K. Chai, N. Ranjbar, M.Z. Jumaat. Damage detection of SFRC concrete beams subjected to pure torsion by integrating acoustic emission and Weibull damage function. Struct. Contr. Health Monit. 2016;23(1):51-69.
[38] BS 8110-1. Structural use of concrete. Code of practice for design and construction. BSI. 1997.
[39] BS 4449. Steel for the reinforcement of concrete. Weldable reinforcing steel. Bar, coil and decoiled product. Specification. BSI. 2005.
[40] ASTM G1-03. Standard Practice for Preparing, Cleaning, and Evaluating Corrosion Test Specimens. American Society of Testing Materials. 2003.
[41] ASTM G31-72. Standard Practice for Laboratory Immersion Corrosion Testing of Metals. American Society of Testing Materials. 2004.
[42] M.A.A. Aldahdooh, N. Muhamad Bunnori. Crack classification in reinforced concrete beams with varying thicknesses by mean of acoustic emission signal features. Constr. Build. Mater. 2013;45:282-288.